Signatures of solar event at middle and low latitudes in the Europe-African sector, during geomagnetic storms, October 2013

Ilyasse Azzouzi, Y. Migoya-Orué, Christine Amory-Mazaudier, Rolland Fleury, S.M. Radicella, A. Touzani

Signatures of solar event at middle and low latitudes in the Europe-African sector, during geomagnetic storms, October 2013

Azzouzi, I[1, 2], Migoya-Orué, Y [3], Amory Mazaudier, C[1,3], Fleury,R[4], Radicella,S,M[3] ,Touzani,A[2].

1. LPP-Laboratory of Plasma Physics /UPMC/Polytechnique/CNRS, UMR 7648, 5 place Jussieu, 75005 France.
2. LA2I/ EMI / University Mohammed V Agdal,Avenue Ibnsina B.P. 765, Rabat, Morocco.
3. T/ICT4D, ICTP - International Centre for Theoretical Physics , Strada Costiera, 11 ,I - 34151 Trieste Italy
4. MO - Dépt. Micro-Ondes//Lab-STICC /UMR CNRS 6285 - Télécom Bretagne Technopole de Brest-Iroise, 29285 Brest, France.
5.
6. Corresponding author: ilyasse.azzouzi@lpp.polytechnique.fr
7. ilyasse.azzouzi@gmail.com

Advances in Space Research (2015), doi: http://dx.doi.org/10.1016/j.asr.2015.06.010

Abstract:
This paper presents the variability of the total electron content, VTEC, the ROTI index (proxy of the scintillation index) and the transient variations of the Earth's magnetic field associated to the impacts of solar events during October 2013. The observations are from middle and low latitudes in European African longitude sector. During October 2013, there are four solar events reaching the Earth. The two first events, on October 2 and October 8 are CME, the third event on October 14, is a jet of fast solar wind flowing from a solar coronal hole, and the last event on October 30 is a slow solar wind with southward excursions of the Bz component of the Interplanetary magnetic field, associated to CME passing near the Earth. For the four events, the variation of VTEC at middle latitudes is the same and presents an increase of VTEC at the time of the impact followed by a decrease of VTEC, lasting one or several days. At low latitudes, no clear common pattern for all the events appears. For the four events the variation of the ROTI index over Africa is different showing the asymmetry between West and East Africa. For the first event, on October 2, the scintillations are not inhibited, for the second and the fourth events on October 8 and 30, the scintillations are inhibited on East Africa and for the third event (high speed solar wind stream), on October 14, the scintillations are inhibited over the whole Africa. The available data allow the full explanation of the observations of October 14, indeed, on this day, there is no post sunset increase of the virtual height h'F2 at Ascension Island. There is no Pre Reversal Enhancement (PRE) of the eastward electric field; it is this electric field which moves up the F layer, the necessary condition for the existence of scintillation. The analysis of the variations of the Earth's magnetic field at low latitudes highlights the presence of the ionospheric disturbance dynamo on October 14, which produces a decrease of the Equatorial Electrojet, several hours after the impact of the high speed solar wind. The disturbance dynamo electric field (DDEF) is westward during the day and till after sunset and turns eastward around 22.30LT. So, on October 14, the westward DDEF inhibits the eastward regular electric field.

Key words: Ionosphere - GPS_TEC - GPS_ROTI- CME- solar wind- coronal hole- geomagnetic storm

1. Introduction

In this paper we present the behavior of VTEC, ROTI index, virtual height h' of the F_2 layer and transient variations of the Earth's magnetic field observed at middle and low latitudes during various solar events (CME, high speed solar wind or event with southward excursion of the Bz component of the Interplanetary magnetic field, IMF). The data used were recorded in Europe Africa longitude sector.

The equatorial ionosphere presents some morphological particularities: 1) the existence of the equatorial ionization anomaly, EIA (Namba and Maeda, 1939; Appleton, 1946), 2) the existence of an ionospheric electric current flowing along the magnetic equator, the equatorial electrojet (EEJ) (Chapman, 1951) and 3) the existence of irregularities of plasma (Basu and Basu, 1981) which disturb the propagation of the electromagnetic signals and as a consequence disturb the GNSS signals. The electric field is the main parameter of the dynamics of the equatorial region and it strongly influences the development of the EIA as well as the Equatorial electrojet and plasma irregularities.

During quiet magnetic periods, the EEJ flows along the magnetic equator. The EEJ is an eastward ionospheric electric current, in the E region, created by the ionospheric dynamo process (Stewart, 1882; Chapman and Bartels, 1940). Its amplitude is 2 times higher than the amplitude of the regular ionospheric currents at middle latitudes (Mazaudier and Blanc, 1982) which generates the Sq variation. The stronger amplitude of the EEJ is due to the existence of a reinforced conductivity at the equator, the conductivity of Cowling. The Cowling conductivity is the combination of Hall and Pedersen conductivities, but the EEJ is mainly an Eastward Hall current (Forbes, 1981; Onwumechili, 1997).

Also, during magnetic quiet periods the regular electric field is generated by the ionospheric dynamo. During the daytime the east–west electric field and the north–south geomagnetic field produce the lift of plasma in E ionospheric region by vertical E X B drift. At higher altitudes in F region, the plasma diffuses downward along the geomagnetic field lines into both hemispheres under the influence of gravity and pressure gradients, this produces the EIA which is characterized by an electron density trough at the magnetic equator, and two crests of enhanced electron density at about ±15 degrees magnetic latitudes.

Another important phenomenon of the equatorial ionosphere is the existence of an increase in the zonal electric field post sunset, the prereversal enhancement (PRE) which causes a strong upward vertical drift (Vz), and a rapid rise up of the F layer. This fact leads to the creation of irregularities in the plasma density (Kelley et al., 2009). The first observations of this large upward vertical drift were made by Woodman (1970) with the incoherent scatter sounder of Jicamarca. Depending on the scale size irregularities, different observations are made, "*the meter scale size irregularities producing plumes in the VHF backscatter radar maps, the decameter sizes that give rise to the spread F echoes in the ionograms, and the hectometer to kilometer sizes produce VHF and UHF radio wave scintillation (Abdu et al., 1983)*". Recently, Chatterjee and Chakraborty (2013) and Chatterjee et al. (2014) studied the scintillations near the crest of the EIA in India, during quiet magnetic days; in their work, they connected EIA, EEJ and scintillations. They found that a post sunset enhancement of the TEC and afternoon enhancement in EEJ are good precursors for postsunset occurrence of scintillation.

During magnetic disturbed periods, the equatorial ionosphere is strongly influenced by auroral phenomena and as a consequence the equatorial electric field is disturbed. Two main disturbance processes are well known 1) the prompt penetration of the magnetospheric electric field, PPEF (Vasyliunas, 1970; Fejer, 1983; Mazaudier et al., 1984; Mazaudier,1985) and 2) the disturbance dynamo electric field, DDEF (Blanc and Richmond , 1980; Fejer, 1983; Sastri, 1988; Mazaudier and Venkateswaran, 1990), related mainly to the Joule heating

produced by auroral electrojets (Testud et al., 1975). The PPEF and DDEF disturb the ionospheric electric currents systems and as a consequence produce magnetic disturbance observed with ground magnetometers. The magnetic disturbance associated to the PPEF is the DP_2 (Nishida et al., 1996; Nishida, 1968) and the one associated to the DDEF is the Ionospheric disturbance Dynamo, D_{dyn} (Mayaud, 1980 ; Fambitakoye et al., 1990; Le Huy and Amory Mazaudier 2005). The main features of the magnetic disturbance associated to the DDEF are an anti Sq circulation at low latitude and a reverse electrojet at equatorial latitudes. Theoretical studies of D_{dyn} (Blanc and Richmond, 1980; Fang et al., 2008; Zaka et al., 2011a and 2011b) reproduced the anti Sq circulation and a reverse EEJ.

In this paper we analyzed the crucial parameters necessary to understand the impact of solar events on Equatorial ionosphere, VTEC, the ROTI index as a proxy of scintillation, the virtual height h' of the F2 in order to know the existence or non existence of PRE of the vertical drift, and the transient variations of the Earth's magnetic field in order to know the presence or not of the PPEF and DDEF.

The second part of the paper is devoted to the data sample and data processing, the third part presents the results, and then there are the discussion and the conclusion.

2. Data Sources and Data processing

2.1 Data sources

We analyze the signature of solar events on ionospheric ionization and Earth's magnetic field during October 2013.

The satellite data from SOHO are used to determine the existence of CME and coronal hole recorded at the surface of the sun www.nasa.gov/mission_pages/soho/, and some informations from the space weather website http://spaceweather.com to determine the solar events reaching the Earth. The solar wind speed and Bz component of the Interplanetary magnetic field (IMF) recorded on board the satellite ACE (http://omniweb.gsfc.nasa.gov /) are used to characterize ~~of~~ the solar wind.

The magnetic indices SSC, Hsym, AU, AL, AE, Kp and Am/Km are extracted from Data Analysis International Union of Geodesy and Geophysics (IUGG) website (http://www.iugg.org/IAGA/). The Storm Sudden Commencement (SSC) indicates the time of arrival of the shock of the CME on the magnetosphere. The Hsym index allows to know the magnetospheric electric currents. The AU and AL indices give the amplitude of the eastward and westward auroral electrojets and the AE index gives an estimation of the energy of the storm. The Am magnetic indices are used to select magnetic quiet days [Mayaud, 1980; Menvielle et al., 2011]. We select for this study very quiet days with all the Km < 2- . We used also the polar cap index which is proxy of the merging electric field $E_M=V_{SW}\ B_T\ \sin^2(\theta/2)$, where V_{SW} is solar wind velocity and B_T ($B_T=(B_Y^2+B_Z^2)^{1/2}$) the transverse component of the interplanetary magnetic field (IMF) in the solar wind. The field direction is represented by the polar angle θ of the transverse component of the IMF with respect to the direction of the Z-axis in a "Geocentric Solar Magnetospheric" (GSM) coordinate system (i.e., $\tan(\theta)=|B_Y|/B_Z$, $0\leq\theta\leq\pi$), (Stauning, 2012).

The ionogram and virtual height recorded at Ascension Island are from the website http://car.uml.edu/common/DIDBFastStationList, and the raw data of the Total Electron Content from the 46 GNSS stations over Africa, middle East—and Europe are used to approach VTEC values and GPS Scintillations. The observatories from AMBER (Yigenzaw et al., 2009) and INTERMAGNET networks provide the variations of the Earth's magnetic field

in various geomagnetic locations. Table 1 gives the geographic and geomagnetic coordinates of the GPS stations magnetic observatories, ionosonde of Ascension Island and magnetometers. Figure 1 is the map of all the observatories.

2.2 Data processing

2.2.1 Data processing of GPS to obtain VTEC and ROTI

We used a standard procedure for processing GPS measurements (Hoffmann-Wellenhof et al . 1992, Schaer, 1999).

The pseudo-range between a GPS satellite and a receiver is the sum of many contributions (1) as follows:

$$P_r^s(f) = \rho_r^s + c.b_r(f) - c.b^s(f) + T_r^s + I_r^s(f) + \alpha_r^s(f) \quad (1)$$

where

ρ_r^s is the slant geometric distance,

$c.b_r$ is the sum of the receiver and clock offset,

$c.b^s$ is the sum of satellite bias and clock offset,

T_r^s is the tropospheric delay,

I_r^s is the Ionospheric delay,

α_r^s is other contributions (relativistic effect, multipaths, …).

On the first order, the ionospheric path delay depends of the slant TEC and of the reciprocal square of the frequency.

$$I_r^s(f) = \frac{a.STEC}{f^2} \quad (2)$$

For dual frequency pseudo-range, we can make the difference between the two measurements which eliminate the geometric and tropospheric terms

$$P_r^s(f_1) - P_r^s(f_2) = \Delta b_r - \Delta b^s + C_i.STEC + \varepsilon \quad (3)$$

The last term ε of the equation is assumed to be negligible for elevation above 10°.

Δb^s is the differential code bias (DCB) of the satellite. We use the monthly values published by the University of Bern.

Δb_r is the differential code bias of the receiver. This receiver bias is a real number known if the receiving station is in a network (IGS, EUREF). The receiver bias is in the files DCB given by CODG. If the receiver is not in a network as DKHL, the receiver bias is unknown and we have to compute it. To remain as easy as possible in its determination, we calculate the STEC with the ionospheric values of CODE/ CODG (Centre for Orbit Determination in Europe ftp.code.com/aiub/CODE) for all Pierce points above an elevation angle cutoff of 30° to eliminate gradients effects. The mean daily difference of the two series of STEC gives the receiver bias (Komjathy et al., 2005).

For the conversion of slant TEC to vertical TEC, we use the single layer mapping function [Schaer,1999]

$$STEC = VTEC\sqrt{1-[\frac{R_T}{R_T+h_m}\cos(E)]^2} \quad (4)$$

where R_T is the earth radius, h_m is the reference altitude taken at 400 km and E the elevation angle.

At each time, we smooth all the VTEC points with a reciprocal square of the elevation angle to give a single value.

The relative STEC is calculated over 30s interval by the combination of phase measurements. We computed the ROT index in units of TECU/min as follows:

$$ROT = \frac{STEC_{k+1} - STEC_k}{time_{k+1} - time_k} * 60 \quad (5)$$

ROTI index is then computed each 30s, by taking the standard deviation of ROT (Pi et al., 1997) over a period of 10-min and with a minimum of 10 points, i.e.

$$ROTI = \sqrt{\langle ROT^2 \rangle - \langle ROT \rangle^2} \quad (6)$$

The ROTI is use to get information of irregularities in the F-region.

The mean averaged quiet TEC : <TEC> computed as the mean arithmetic value of quiet magnetic days of October 2013.

$$<\text{VTECquiet}> = \frac{1}{n}\sum_{i=1}^{n}(\text{VTECquiet})i \quad (7)$$

where i equal 1,…13, there are 13 quiet days in October 2013.

2.2.2 Data processing of magnetometers data

The mean averaged quiet ΔH component of the Earth's magnetic field is computed following the same equation of (7) :

$$<\Delta\text{Hquiet}> = \frac{1}{n}\sum_{i=1}^{n}(\Delta\text{H}quiet)i \quad (8)$$

where i equal 1…13.

Table 2 gives the Am value of the quiet days of October selected to establish the magnetic quiet time level.

The magnetic disturbance due to ionospheric electric currents is computed by the following expression given by Le Huy and Amory-Mazaudier (2005):

$$\text{Diono} = \Delta\text{H} - \text{Hsym}.\cos\lambda - <\Delta\text{Hquiet}> \quad (9)$$

H is the component of the magnetic field recorded in one station

Hsym is an estimation of the ring current

λ is the geomagnetic latitude

$$\text{Diono} = \text{DP2} + \text{Ddyn} \quad (10)$$

DP_2 is the magnetic disturbance related to the prompt penetration of magnetospheric electric field (Nishida, 1968; Vasyliunas, 1970)

D_{dyn} is the magnetic disturbance related to the ionospheric disturbance dynamo (Blanc and Richmond, 1980; Mazaudier and Venkateswaran, 1990; Le Huy and Amory-Mazaudier, 2005)

To separate the effect of the DP_2 signal from the disturbance dynamo (D_{dyn}) signal, we used the method develop by Fathy et al., 2014 . Fathy et al., 2014 remove the DP_2 signal by taking the average value of 4 h with sliding of 1 h, and MATLAB programs (interpolation, average, and mean).

3. Results

3.1 The four events of October 2013

We analyze the month of October 2013, SOHO (SOlar and Heliospheric Observatory) solar data shows that several CME are ejected during this period. Three CME hits the Earth during October 2013. The SSC data give the time of the shock of the CME (http://www.iugg.org/IAGA/). The first CME hits the Earth in the early morning on October 2 (SSC : "Sudden Storm Commencement" at 01.55 UT), the second one on October 8 in the evening (SSC at 20.22UT) and the third one on October 15 at 10.00UT, for this last event there is no detectable SSC. Several other CME swept the Earth on October 29 and 30. During this same period there is also the arrival of high speed solar wind associated to a solar coronal hole on October 14 around 08.00UT. Figure 2 gives a global view of the month of October with 4 events. From the top to the bottom the plots correspond to the solar wind speed, the Bz component of the Interplanetary Magnetic Field (IMF), Hsym and the AU and AL magnetic indices. The start of each event is indicated by a red line on the Hsym curve.
Figures 3a, 3b, 3c and 3d are similar to figure 2 and give a zoom of each event.
On the top panel of figure 3a, the solar wind speed increases on October 2 at 02.00UT from 400km/s to 600km/ at the time of the SSC (01.55UT). It is the time of the shock of the CME on the magnetosphere. At the same time, on the second panel, a strong oscillation of the Bz component of the IMF occurs. The IMF Bz becomes several times negative ,-10nT at 01.55,-20nT at 02.30UT ,- 12 at 03.00 and -35nT at 04.10UT. The third panel shows the variation of the magnetic index Hsym, the blue line indicates the SSC. The Hsym increases to + 50 nT when the CME hits the Earth, and then decreases to -35 nT around 03.00UT, increases again and decreases to the value of -79nT around 05.50UT. The last panel reproduces the AU and AL magnetic indices, we observe on October 2, ~~2~~ two large increases of AU and AL indices associated the Hsym decreases, at 01.55UT AU decreases to -1000 nT and AL increases to 600nT, at 03.00 UT AU decrease to -1500 nT and AL increases to 850 nT and finally around 06.00UT AU decreases to -1400 nT and AL increases to 500nT. We can notice that during the night from October 2 - 3, the auroral activity is very weak.

The second case is rather similar to the first one. On the top panel of figure 2b, the solar wind increases on October 8th at the end of the day from 300km/s to 700km/s, when there is the impact of a CME at 20.22UT. The solar wind speed increases in several steps and reaches its maximum value 700km/s on October 9 around 08.00UT. On the second panel, there is the Bz component of the IMF associated to this event, which becomes negative at 20.20UT (Bz= -10nT), 21.30UT (Bz= -34nT) and 23.00UT (Bz= -12nT). The third panel shows the variation of the magnetic index Hsym, the blue line indicates the SSC. The Hsym decreases to -70 nT when the CME hits the Earth, then increases and decreases again to reach the minimum value -75nT at 00.30UT on October 9th.
The last panel reproduces the AU and AL magnetic indices; AU reaches a maximum value around 1000 nT around 22.30UT . For this case during the night Octobre 8-9, the auroral activity is not negligible, the AU index maximum is around 500 nT.
On the top panel of figure 3c the solar wind speed increases on October 14 around 08.00UT, from 300 km/s to 550km/s .This increase is related to the arrival of high speed solar wind

stream associated to a coronal hole. A second disturbance arrives on October 15th at 10.00UT associated to CME hitting the Earth with no SSC. On the second panel the Bz component of the IMF oscillates, this is a common feature of solar wind stream associated to coronal hole; there is no strong oscillation as for the 2 previous events. The third panel of figure 3c shows the variation of the magnetic index Hsym. Hsym decreases slowly and reached the minimum value -50nT around midnight. The last panel reproduces the AU and AL magnetic indices; we observe that there is an increase of AU and AL indices associated to coronal hole. There is no strong burst of the AU index as for the 2 previous cases. The AU is ~ – 500nT during the whole October 14 and during the morning on October 15, with some peaks of 800nT to 1000 nT.

For the fourth event, there is no major disruption. On the top panel of figure 3d, the solar wind is slow below 400km/s during the whole period except on October 31. On the second panel the Bz component of the interplanetary magnetic field is negative during large periods on October 29 and 30 associated with a CME passing near the Earth. On October 30 Hsym decreases in 2 steps and reaches the minimum value of 50nT around midnight. On the last panel, the AU and AL indices show a disturbance starting in the morning on October 30 and lasting until midnight the same day.

3.2 Along the West-African Europe sector

Figure 4a is composed of five panels corresponding to the VTEC variations observed during October 2013 at different locations of middle and low latitudes. On each panel the red curve represents the regular mean variation based on magnetic quiet days and computed following the equation 7 and the blue curve the variations of the VTEC observed.

The 2 first panels at the top, corresponding to middle latitudes stations of VIGO and LAGO exhibit the same pattern: the VTEC increases at the arrival of the disturbance (CME, high speed solar wind streams, or glance of CME) and decreases on the days after. Shimeis et al. (2012) observed the same pattern at Helwan in Egypt for a CME hitting the Earth on April 5, 2010. The depletion of VTEC is observed during several days. For the first event, the depletion of VTEC is observed on October 3, 4, 5 and 6. For the second event the depletion is observed on October 9 and 10. For the third event the depletion is observed on October 15 and 16. Finally for the fourth event there is a decrease on October 31.

We have to notice here that for the second event the increase of VTEC is not significant due to the fact that there is a strong disturbance before.

For the first and second event [October 2, October 8], at MAS1 and DKHL (panels 3 and 4 from the top) there is no significant increase of the VTEC at the beginning of the disturbance and no decrease on the days after. On the contrary we observe an increase of VTEC on the days after the events, on October 4 and October 10, 11 and 12. For the third and fourth events [October 14 and October 30], we observe the same pattern than at VIGO and LAGO: an increase of VTEC on the starting day [October 14, October 31] and a decrease on the day after [October 15 and October 31], but the amplitudes of the variations of VTEC is smaller than those observed at Vigo and Lago. At MAS1 and DKHL, there are strong VTEC on October 22, 23, 24 and 25.

Finally on the bottom panel of figure 4a at the station DAKR at low latitudes there is no significant variations of VTEC associated to these 4 events.

Figure 4b illustrates the variations of the VTEC in relation with the median VTEC, for the stations presented in figure 4a. For each time, we calculate the difference between the daily VTEC and the VTEC median, and then we compute the average value of each day. The average value thus reflects the daily average deviation from the median. The vertical lines

represent the standard deviation (rms) of this variation. For a given day the vertical line lenght gives the difference between the VTEC of the day and the median VTEC. At LAGO and VIGO (top panels), we clearly see the increases and depletions of VTEC for all the events. At the other stations MAS1, DKHL and DAKR, the signatures of the events are not clear and the error bars are greater.
Figure 5 shows the maps of ROTI for the 4 selected events, these maps are made by using the algorithm described in equations 5 and 6. The ROTI index was calculated for 46 GPS stations and 46 geographic positions between the longitudes 30 W and 60 E. On the background coast mapping, we plotted these indices following the coordinates of Pierce points with two color codes: 1) thin ~~waist,~~ gray when the value of ROTI is less than 1.5tecu/min and 2) red square~~,~~ of greater dimension, when the ROTI index exceeds 1.5tecu/min.
All daily points were keeping when the elevation angle is greater than 15 ° to eliminate the possible effect of multipath at low angles. The magnetic dip equator is calculated from the IGRF coefficients for the month of October 2013 and is plotted on the graphs by the solid line in cyan. The choice of maximum stations can cover three major areas in the West, Centre and East Africa over several tens of degrees of latitude. Unfortunately, the lack of measures in some large regions not ensures the spatial continuity of representation.
In Figure 5, the 2 top panels correspond to the first event [October 2-3], we observe the same pattern of scintillations for October 2 and 3. The arrival of the CME on October 2 at 01.55UT does not change the pattern of scintillations during the 2 days.
On the contrary, the 2 following panels corresponding to the second event [October 8-9] show that on October 9 the day after the arrival of the CME, scintillations disappear on East Africa.
The 2 following panels, devoted to the third event [October 14 -15], highlight the disappearance of the scintillation on October 14, over all Africa. On October 15 the scintillations are again observed across Africa.
The 2 bottom panels concerning the fourth event [October 30-31] show that scintillation disappears only on East Africa during the 2 days.
From the 31 daily graphs (not shown here), we can make the following observations:
- Strong ROTI indices are mainly positioned at 15 ° magnetic latitudes, on each side of the magnetic dip equator. Their spatial extension is about 8-12 degrees of latitude,
- Maximum red points (ROTI index exceeding 1.5tecu/min) occur on October, 8,
- In East Africa, between 09-14 October and on October 30, an almost total disappearance of strong values of ROTI index is observed,
- In West and Central Africa, disappearance of strong values of ROTI only takes place only one day, on October 14.

Figure 6 is composed like the figure 4a by 6 panels corresponding respectively from top to bottom to the stations VIGO, LAGO, MAS1, DKHL, DAKR and NKLG. All the stations are located in West Africa. On each panel are superimposed the Kp index (red line) and the ROTI in green color, for the whole month of October.
At VIGO there is no scintillation and at LAGO a very low level of scintillations is observed during very few days. This fact is explained by the location of these stations at middle latitudes. At the stations MAS1, DKHL, DAKR and NKLG, strong scintillations are observed all the days except on October 14. We observe a decrease of the amplitude of scintillations on October 30 at DAKR and NKLG.

Figure 7 presents ionograms recorded at Ascension Island during the four events. All the ionograms are recorded at 22.45UT. The top left corresponds to October 2, the top right

panel to October 8, the bottom left panel to October 14 and the bottom right panel to October 30.
On October 2 and 30 we observe a moderate spread F, on October 8, a very strong spread F and on October 14 no spread F.

Figure 8 illustrates for the four events the variation of the virtual height of the F2 layer at 4MHz recorded at Ascension Island. On each panel the black line is the median. The common behavior for all the days is an increase of the virtual height from 15.00UT to 17.30UT to a value of 260km. Then the virtual height decreases until 19.00UT and increases again to reach a maximum value between 260km and 300 km around 20.00UT or 21.00UT depending on the day.

There is only one day, October 14, which exhibit another pattern, indeed the virtual height is always at the same altitude from 17.00UT to 21.00UT around 240 km height.
Another particularity is observed on October 2nd the virtual height oscillates and presents 3 maxima [270 km at 17.15UT, 260km at 20h00 UT and 260 km at 23h30 UT], this behavior reveals the existence of a gravity wave (Testud et al., 1975).

Figure 9 illustrates the Earth's magnetic variations from October 13 to October 17. From the top to the bottom there are successively the PC index, the AE index and the variations of the Earth's magnetic field along a latitudinal magnetic chain of six magnetometers. Four magnetometers are from the INTERMAGNET network (UPS, CLF, TAM and MBO) and two magnetometers are from the AMBER network (CNKY, CMRN). At the observatories UPS, CLF, TAM, MBO and CMRN, the regular variation of the Earth's magnetic field computed by using the equation 7 (red curve) is superimposed the observations recorded (blue curve). At the observatory of Conakry we used to estimate the regular variation the observation made on ~~the~~ October 13, the magnetic quiet day preceding the event, as there are many gaps in the data during magnetic quiet days of the month.

Around 08.00UT when the solar wind increases (see figure 2), the PC and AE indices simultaneously increase, revealing the transfer of energy and momentum from the solar wind to the magnetosphere. These two magnetic indices present also many oscillations. At Uppsala and Chambon La Foret, we observe the same pattern with an increase of the H component, around 08.00UT, related to the increase of the solar wind speed. Several hours after the H component decreases, we notice also the presence of strong oscillations. These oscillations are the signature of the DP_2 current system (Nishida et al., 1966 ; Nishida, 1968) related to the prompt penetration of magnetospheric convection electric field, PPEF.

The observatories of TAM, MBO, CNKY and CMRN exhibit the same behavior. During the morning the H component follows the regular variation and presents oscillations. Then the H component decreases and remains smaller than the regular variations on October 15.
We computed the magnetic disturbance related to the ionospheric electric current disturbance Diono, [$DP_2 + D_{dyn}$] by using equation 9. This disturbance is presented by the red curve on the figure 10. The blue curve on figure 10 is an estimation of the magnetic signature, D_{dyn} of the electric current disturbance due the sole ionospheric disturbance dynamo, DDEF (Fathy et al., 2014). This signature is reversed to the normal diurnal Sq current system related the solar radiation (Chapman, 1940). From the figure 10 we can conclude that the ionospheric disturbance dynamo (blue line) is acting on October 14, its

amplitude around – 28 nT is significant. On October 15 and 16, its amplitude is smaller around – 10 nT.

3.3 Along the East-African-Europe/Middle East sector

Figure 11 is similar to figure 6 and corresponds to East Africa. On the top panel, at the station RAMO, there are few scintillations. The amplitude of scintillations is greater than 3, on October 3, 15 and 18; October 3 and 15 are the days after the first and the third event.
At NAMA, ARMI, DODM and MZUZ, the scintillations disappear from October 9 to October 14. At ARMI, the scintillations are weaker than at NAMA, DODM and MZUZ. We can also observe the disappearance of the scintillations at NAMA, DODM and MZUZ on October 30 and 31. Finally at ZOMB, there are no large scintillations, except on October 21.
The comparison of figures 6 and 11 highlights the asymmetry in scintillation behavior between East and West Africa during October 2013.
In East and Middle East Africa, it was not possible to develop the same analysis than in West Africa due to the fact that there are no ionosonde data and no AMBER and INTERMAGNET magnetometers data available during this event.

4 Discussion

In this paper we analyze crucial parameters of the middle and low latitudes during 4 different solar events. Unfortunately due to the lack of data over East Africa we will concentrate our study on West Africa.
In figures 2 and 3 devoted to the solar wind parameters and the magnetic indices Hsym, AU and AL, we see that the 2 first events are rather similar. The first event is a CME impacting the Earth in the early morning on October 2nd at 01.55UT, and the second event, a CME impacting the Earth in the evening on October 8 at 20.55UT. At middle latitudes, the two CME produce the same perturbation of VTEC (figures 4a and 4b): an increase of the VTEC during the impact and after a decrease of VTEC which can last one day or more.

The two other events are different. The third event is the impact of high speed solar wind on October 14 at 08.00UT and the fourth event is related to a slow solar wind with southward Bz on October 30. They produce also the same signature at middle latitudes. These results are similar to those obtained by Shimeis et al. (2012) and can be explained by the successive action of PPEF at the beginning of the event and DDEF several hours later.
At low latitudes there is not a clear common signature for all the events.
Figure 5 shows the maps of the ROTI index, a proxy of scintillation. The signature is different from one case to another. The impact of the first CME does not produce any change in the scintillation pattern on October 2nd and 3rd (top panels, Figure 5) .The impact of the second CME produces the disappearance of scintillations on East Africa (second panels from the top, Figure 5). On October 14, the day of arrival of the high speed solar wind stream (third panels from the top, Figure 5); the scintillations disappear over all Africa. Finally for the last event, CME passing near the Earth (bottom panel, Figure 5); the scintillations disappear on East Africa.

Figures 6 and 11 show the variations of the ROTI index for several stations in West Africa (figure 6) and East Africa (figure 11). There is an asymmetry between West and East Africa depending of the event. Indeed for the events of October 2nd and October 14 the whole

Africa exhibits the same pattern for scintillation, i.e no inhibition of scintillation on October 2nd and inhibition of scintillation on October 14. On the contrary for the second and third events, October 8 and October 30, the scintillations disappear only over East Africa. We must also notice that during the second event, over East Africa, the disappearance of scintillations lasts several days from October 9 to October 13.

The fact the scintillation pattern is different from one site to another for the same magnetic event was found previously by several authors. Santos et al. (2012) found strong longitudinal difference in ionospheric responses over Fortaleza (Brazil) and Jicamarca (Peru) during the January 2005 magnetic storm. They found the total suppression of the PRE over Fortaleza with no simultaneous effect over Jicamarca. Jicamarca and Fortaleza locations are separated by only 2 hours in local time. Chatterjee and Chakraborty (2013) noticed that the locations of observing stations with respect to the post-sunset resurgence peak of EIA seem to play dominant role in dictating the severity of scintillation activity.

Over West Africa we have the possibility to interpret the observations with the ionosonde of Ascension Island. In figure 7 are presented the ionograms obtained for the four events, and in Figure 8 the variations of the virtual height h'F2 at 4Mhz. In figure 8, among the 15 days presented, only one day October 14 exhibits a different pattern, i.e the F layer does not present the PRE signature which is an increase of the h' height post sunset. This fact explained the absence of scintillation on October 14.

We know that the lift up of the F layer is related to the existence of the PRE of the eastward electric field. The observations suggest that during the event of October 14 a disturbed electric field inhibits the regular eastward electric field. Two physical processes 1) the Prompt penetration of magnetospheric convection and 2) the ionospheric disturbance dynamo, produce disturbed electric fields. The electric field which penetrates to low latitudes before the shielding becomes effective (undershielding PPEF). This field has the polarity of the dawndusk convection electric field (eastward during the day until 21.00 LT and westward in night sector). The over-shielding electric field (Kelley et al., 1979; Kobea et al., 2000) is related to the decline of the convection electric field. This electric field is westward in the day side and eastward in the night side (PPEF).

Finally the disturbance dynamo electric field, DDEF (Blanc and Richmond, 1980; Sastri, 1988) which is westward during the day, turns eastward around 22.30LT and remains eastward until the end of the night (Huang et al. 2005).

In Figure 9, at low latitudes, the variations of the H component (TAM, MBO, CNKY and CMRN) show before noon strong oscillations, which are the signature of the DP_2 current system related to PPEF (under or over shielding). After noon we observe a decay of the H component of the Earth's magnetic field. This decay occurs several hours after the beginning of the disturbance; it is the signature of the D_{dyn} current system related to DDEF. By using the method of Fathy et al. (2014), we estimated the Diono and D_{dyn} disturbances. Figure 10 illustrates their variations. On October 14, there is the existence of the ionospheric disturbance process which generates a westward electric field during the day until the evening. This electric field inhibits the regular eastward electric field, and as a consequence there is no scintillation.

From October 9 to 13 the scintillations are inhibited over East Africa and not on West Africa. The H component observed at the station CMRN on these days (not shown here) exhibits an afternoon secondary maximum, which is the precursor of scintillation following Chatterjee et al. (2014), and scintillations are observed. Ngwira et al., 2013, studied scintillations in 4 African GPS stations from West to East Africa. During the storm event of September 13 2004, they observed scintillations in all the stations and interpreted this fact as a consequence of

the prompt penetration of an Eastward electric field (PPEF). On the day after the storm, September 14, the scintillations disappeared in 2 stations and they observed a decrease of H component as we observed on October 14, 2013.

5 Conclusion

In this paper we analyzed the impacts on the ionosphere of 4 four different solar events (2two CME, a high speed solar wind flowing from a coronal hole and a slow solar wind associated to large southward excursions of the BZ). We analyzed VTEC data, ROTI index, ionosonde and magnetic data and found the following results:

- At middle latitude for all the events the behavior is similar, an increase of the VTEC at the time of the impact followed by a decrease of the VTEC during one or more days. These observations are explained by the electric field disturbance PPEF (prompt penetration electric field) at the beginning and several hours later by the electric field disturbance DDEF (Disturbance dynamo electric field). Such observations were made recently by Shimeis et al. (2012)
- At low latitudes there is no a clear common signature for all the events.
- The ROTI index which is a proxy of the scintillation index showed that concerning the scintillations, there is an asymmetry between East and West Africa. Indeed, sometimes the scintillations are inhibited only on East Africa (October 9-13 and October 30), sometimes the scintillations are inhibited over the whole Africa (October 14) and there are cases where there is no inhibition of scintillation everywhere in Africa (October 2). Such results were found in the American longitude sector by Santos et al., (2012), and explained by the longitudinal variation of the disturbances PPEF as well as DDEF.

The analysis of the the virtual height h'F2 at 4MHz, recorded by the ionosonde of Ascension Island (West Africa), on October 14 (the day of inhibition of scintillation of whole Africa) showed that there is no uplift of the layer post sunset on October 14, i.e there is no PRE of the eastward electric field and therefore no scintillation.

- The analysis of the ground magnetic variations of the H component at low latitudes, on October 14, showed the existence of PPEF and DDEF electric field disturbances. During the event of inhibition of the scintillation it is a westward DDEF field opposite to the PRE eastward electric field which stopped the uplift of the F layer.

Due to the lack of data, we can fully interpret only the case of inhibition of scintillation over West Africa on October, 14 2013. Indeed, during October 2013, the magnetometers of the 2 networks AMBER and INTERMAGNET, located in East equatorial latitudes, were not working, and there is no ionosonde data available on East Africa. It is important, if we want to develop Space Weather studies in Africa, to increase the number of scientific instruments. An equatorial chain of ionosondes as well as an incoherent scatter sounder would be very useful to understand the longitudinal asymmetry of scintillations.

Acknowledgements

The results about geomagnetic data presented in this paper rely on the data collected at UPS, CLF, MBO and TAM. We thank IPGP, CRAAG and SGU institutes, for supporting its

operation and INTERMAGNET for promoting high standards of magnetic observatory practice (www.intermagnet.org). The authors also thank E. Yizengaw, E. Zesta, M. B. Moldwin and the rest of the AMBER and SAMBA team for the data. AMBER is operated by Boston College and funded by NASA and AFOSR.
The authors thank all the providers of the GPS data of the networks IGS and UNAVCO as well as the National Moroccan Agency for the Land Conservation, Land Registry and Mapping (ANCFCC) ,in charge of the station DKHL in Morocco.
The authors thank Lowell GIRO Data Center (LGDC) and all the providers of the Ascension Island ionograms.
Our sincere thanks go to all members of LPP/Polytechnique/ UPMC/CNRS, Telecom Bretagne-Brest University and Ecole Mohammadia d'Ingénieurs (EMI)/Université Mohammed V Agdal Rabat-Unversity for their ceaseless support .

References

Abdu, M. A. , R. T. de Medeiros, J. H. A. Sobral, and J. A. Bittencourt, Spread F plasma bubble vertical rise velocities determined from space ionosonde observations, Journal of Geophys. Res., vol.88, n A11, pp 9197-9204, 1983.

Appleton, E. Two anomalies in the ionosphere. Nature 157, 691-693, 1946.

Blanc, M., A. D. Richmond , The Ionospheric disturbance dynamo, Journal of Geophys. Res., Vol. 85, N°. A4, pp 1669-1686, April 1, 1980.

Basu, S., and S. Basu, Equqtorial scintillations , a review, Journal of Atmosph. and Terr. Physics, vol.43, n 5/6, pp 473-498, 1981.

Chapman, S. and J. Bartels, Geomagnetism, Oxford University Press, New York, 1940.

Chapman, S., The equatorial electrojet as detected from the abnormal electric current distribution above Huancayo, Peru, and elsewhere, Arch. Meteorol. Geophys. u. Bioklimatol. ser., A, 4, 368-374, 1951.

Chatterjee, S. and S.K. Chakraborty, Variability of ionospheric scintillation near the equqtorial crest of the Indian zone, Ann. Geophys., 31, 697-711, doi:10.5194/angeo-31-697-2013.

Chatterjee, S., S.K. Chakraborty, B. Veenadhari and S. Banola, A study on iomospheric scintillation near the EIA crest in relation to Equatorial Electrodynamics, Journal of Geophys. Res. Space Physics, 119, 1250-1261, doi:10.1002/2013JA019466, 2014.

Fambitakoye O., M. Menvielle, C. Mazaudier, Global disturbance of the transient magnetic field associated to thermospheric storm winds on March 23, 1979, Journal of Geophys. Res., 95, A9, 209-218,1990

Fang, T.W., A. D. Richmond, J. Y. Liu, and A. Maute, Wind dynamo effects on ground magnetic perturbations and vertical drifts, Journal of Geophys. Res., Vol. 113, A11313, doi:10.1029/2008JA013513, 2008.

Fathy, I., C. Amory-Mazaudier, A. Fathy, A. M. Mahrous, K. Yumoto, and E. Ghamry, Ionospheric disturbance dynamo associated to a coronal hole: Case study of 5–10 April 2010. J. Geophys. Res. SpacePhysics, 119, doi:10.1002/2013JA019510, 2014.

Fejer B., M.F. Larsen and D.T. Farley, On the Equatorial disturbance dynamo electric fields, Geophys. Res. Let., vol 10, n°7, 537-540, 1983.

Forbes, J.M., The equatorial electrojet, Rev Geophys Space Phys 19, 469-504, 1981.

Huang, C. M., A. D. Richmond, and M. Q. Chen, Theoretical effects of geomagnetic activity on low latitude ionospheric electric fields, Journal of Geophys. Res.,vol 110, A05312, doi:10.1029/2004JA010994, 2005.

Hofmann-Wellenfof B., H. Lichtenegger, J. Collins, Global Positioning System: theory and Practice, Springer-Verlag, Wien, New-York, 1992.

Kelley, M. C., B. G. Fejer, and C. A. Gonzales , An explanation for anomalous equatorial ionospheric electric fields associated with a northward turning of the interplanetary magnetic field, Geophys. Res. Lett., 6(4), 301–304, doi:10.1029/GL006i004p00301, 1979.

Kelley M.C., R.R Ilma, and G. Crowley, On the origin of the pre-reversal enhancement of the zonal equatorial electric field, Ann. Geophys., 27, 2053-2056, 2009.

Kobea A.T., A.D. Richmond, B.A. Emery, C. Peymirat, H. Luhr, T. Moretto, M. Hairston et C. Amory-Mazaudier, Electrodynamic Coupling of High and Low Latitudes Observations on May 27,1993, Journal of Geophys. Res.,vol 105, N° A10, pages 22979-22989, October, 1, 2000.

Komjathy A., L. Sparks, B.D. Wilson, A.J. Mannucci, Automated daily processing of more than 1000 ground-based GPS receivers for studying intense ionospheric storms, Radio Science, v40, RS6006, doi:10.1029/2005RS003279, 2005.

Le Huy, M. C. Amory-Mazaudier, Magnetic signature of the Ionospheric disturbance dynamo at equatorial latitudes : « Ddyn », Journal of Geophys. Res, Vol 110, A 10301, 2005.

Mayaud, P.N., Derivation, Meaning and Use of Geomagnetic Indices, Geophysical Monograph series, Vol 22, AGU, Washington DC, 1980.

Mazaudier C., M. Blanc, Electric currents above Saint-Santin; Part II: Model, J. Geophys. Res., 87 (A4), 2465-2480,1982.

Mazaudier C., M. Blanc, E. Nielsen, Z. Min-Yun, Latitudinal profile of the magnetospheric convection electric field at ionospheric altitudes from a chain of magnetic and radar data, J. Geophys. Res., 89, (A1), 375-381,1984.

Mazaudier C., Electric currents above Saint-Santin; 3- A preliminary study of disturbances : June 6, 1978; March 22, 1979; March 23, 1979., J. Geophys. Res., 90 (A2), 1355-1366,1985.

Mazaudier C., S.V. Venkateswaran, Delayed ionospheric effects of March 22, 1979 studied by the sixth Coordinated Data Analysis Workshop (CDAW-6), Ann. Geophysicae, 8, 511-518,1990.

Menvielle, M., T. Iyemori, A. Marchaudon, M. Nosé, Geomagnetic indices, in Geomagnetic Observations and Models, Menvielle, M., T. Iyemori, A. Marchaudon, M. Nosé, Geomagnetic indices, in Geomagnetic Observations and Models, Mandea M. , Korte, Monica (Eds), Special Sopron Book Series 5, DOI 10.1007/978-90-481-9858-0_8, Springer Dordrecht Heidelberg London New York, 2011.

Namba, S., Maeda, K.-I. Radio Wave Propagation. Corona Publishing,Tokyo, p. 86, 1939.

Ngwira, C.M., G.K. Seemala, J.B. Habarulema, Simultaneous observations of ionospheric irregularities in the African low latitude region, Journal of Atmospheric and Solar Terrestrial Physics, 97, pp 50-57, 2013.

Nishida, A., Iwasaki N., and N. T. Nagata, The origin of fluctuations in the equatorial electrojet: A new type of geomagnetic variation, Ann. Geophys., 22, 478-484, 1966.

Nishida, A., Geomagnetic DP_2 fluctuations and associated magnetospheric phenomena, J. Geophys. Res., 73, 1795– 1803, 1968.

Onwumechili CA, The Equatorial Electrojet. Gordon and Breach Science Publishers, The Netherlands, Amsterdam, 1997.

Pi X. ,A.J. Mannucci, U.J. Lindqwister, C.M. Ho, Monitoring of global ionospheric irregularities using the worldwide GPS network, Geophysical Research Letters, v24, pp2283-2286, 1997.

Santos, A.M., M.A. Abdu, J.H.A. Sobral, D. Koga, P.A.B. Nogueira , C.M.N. Candido : 2012, Strong difference in ionospheric responses over Fortaleza (Brazil) and Jicamarca (Peru) during the January 2005 magnetic storm dominated by northward IMF, , J. Geophys. Res. , vol 117, A08333, doi: 10.1029/2012JA0117604.

Sastri, J.H., Equatorial electric field of Ionospheric disturbance dynamo origin Annales Geophysicae, 6, (6), 635-642, 1988.

Schaer, S., Mapping and predicting the Earth's ionosphere using the Global Positioning System, Ph.D. thesis, 228p, Bern University, Bern, 1999.

Shimeis, A., I. Fathy, C. Amory-Mazaudier, R. Fleury, A. M. Mahrous, K. Yumoto, and K. Groves, Signature of the coronal hole near the north crest equatorial anomaly over Egypt during the strong geomagnetic storm 5 April 2010, J. Geophys. Res., 117, A07309, doi:10.1029/2012JA017753, 2012.

Stauning, P., The Polar Cap PC Indices: Relations to Solar Wind and Global Disturbances, Exploring the Solar Wind, Dr. Marian Lazar (Ed.), ISBN: 978-9 53-51-0339-4, InTech, 2012 Available from:

http://www.intechopen.com/books/exploring-the-solar-wind/the-polar-cap-pc-indices-relations-to-solar-wind-and-global-disturbances

Testud, F., P. Amayenc, and M. Blanc, Middle and low latitude effects of auroral disturbances from incoherent scatter, J. Atmos. Terr. Phys., 37, 989-1009, 1975.

Stewart, B., Terrestrial magnetism, in Encyclopaedia Britannica, 9th ed., vol. 16, p. 159, 1882.

Vasyliunas, V. M., Mathematical models of magnetospheric convection and its coupling to the ionosphere, in Particles and Fields in the Magnetosphere, edited by M. McCormac, Springer, New York , pp 60 – 71, 1970.

Woodman, R. F. , Vertical drift velocities and east-west electric fields at the magnetic equator. *J. Geophys. Res.* **75**, 6249-6259, 1970.

Yigenzaw, E., and M. B. Moldwin, African Meridian B-field Education and Research (AMBER) Array, Earth Moon Planet,104(1), 237-246, doi:10.1007/s11038-008-9287-2, 2009.

Zaka, K.Z., A.T. Kobea, V. Doumbia, A.D. Richmond, A. Maute, N.M. Mene, O.K. Obrou, P. Assamoi, K. Boka, J.-P. Adohi, and C. Amory-Mazaudier, Simulation of electric field and current during the 11 June 1993 disturbance dynamo event: Comparison with the observations, J. Geophys. Res., 115, A11307, doi:10.1029/2010JA015417, 2010a.

Zaka, K.Z., A.T. Kobea, V. Doumbia, A.D. Richmond, A. Maute, N.M. Mene, O.K. Obrou, P. Assamoi, K. Boka, J.-P. Adohi, and C. Amory-Mazaudier, Correction to "Simulation of electric field and current during the 11 June 1993 disturbance dynamo event: Comparison with the observations," J. Geophys. Res., 115, A12314, doi:10.1029/ 2010JA016292, 2010b.

Table captions

Table 1 Geographic and Geomagnetic coordinates of the GPS stations, magnetometers and ionosonde.
Model IGRF 2013 "International Geomagnetic Reference Field " (http://wdc.kugi.kyoto-u.ac.jp/igrf/gggm/index.html)

Table 2: Am values of the magnetic quiet days used to determine the magnetic quiet reference level

Figure captions

Figure 1: map of the GPS, the magnetometers and the ionosonde of Ascension Island

Figure 2: The solar wind parameters and geomagnetic indices for October 2013: (a) Vp the speed of the solar wind in km/s, (b) the Bz component of the interplanetary magnetic field, (c) the Hsym index and (d) the AU and AL indices.

Figure 3: The solar wind parameters and geomagnetic indices for the 4 Periods of October.

Figure 4a: VTEC along the West-African Europe sector during October 2013
Figure 4b: Daily average deviation of VTEC from the median VTEC.

Figure 5: Maps of Tracks of GNSS satellites, around the observing stations for the events of October 2013. Pseudorandom noise (PRN) codes of the satellites and scintillation timing of the corresponding L1 band scintillation are provided for each track (read color).

Figure 6: ROTI and Kp indices, along the West-African Europe sector during October 2013

Figure 7 : Ionogram of Ascension Island for 02,08,14 and 30 October 2013, at 15h and 20h (UT +1)

Figure 8 : Variations of the virtual height h'F2 layer during October 2013, between 15h and 24h, every 15 minutes at 4 MHz in Ascension Island (UT +1). Each panel corresponds to an event.

Figure 9: PC, AE magnetic indices and H component of the Earth's magnetic field along a latitudinal magnetic chain.

Figure 10 : Disturbances of Ionospheric currents D_{iono} and D_{dyn} at M'BOUR observatory , Senegal

Figure 11 : ROTI and Kp indices, along the East-African-Europe/Middle East sector, during October 2013

Table 1 Geographic and Geomagnetic coordinates of the GPS stations, magnetometers and ionosonde.
Model IGRF 2013 "International Geomagnetic Reference Field " (http://wdc.kugi.kyoto-u.ac.jp/igrf/gggm/index.html)

	Id	City	Location	Geographic (decimal degrees)		Geomagnetic (decimal degrees)	
				Longitude (negative for west)	Latitude (negative for south)	Longitude (E)	Latitude (N/S)
GPS Stations	ARMI	Arba Minch	Ethiopia	37.56 E	6.06 N	110.72	2.61 N
	DAKR	DAKAR	Senegal	17.46 W	14.68 N	57.54 E	20.05 N
	DKHL	Dakhla	Morocco	15.94 W	23.68 N	30.63 E	28.67 N
	DODM	Dodoma	Tanzania	35.73 E	6,17 S	106.94 E	9.09 S
	LAGO	Lagos	Portugal	8.66 W	37.09 N	71.09 E	40.68 N
	MAS1	Maspalomas	Gran Canaria Spain	15.63 W	27.76 N	61.73 E	32.63 N
	MZUZ	Mzuzu	Malawl	34.00 E	11.42 S	104.33 E	13.95 S
	NAMA	Namas	Saoudi Arabia	42.04 E	19.21 N	117.19 E	14.81 N
	NKLG	Libreville	Gabon	9.67 E	0.35 N	82.30 E	1.68 N
	RAMO	Mitzpe Ramon	Israel	34.76 E	30.59 N	112.30 E	17.09 N
	VIGO	Vigo	Spain	8.81W	42.18 N	72.40 E	45.68 N
	ZOMB	Zomba	Malawi	35.33E	15.38S	105.17E	18.05S
Magnetometers	UPS	Uppsala	Sweden	17.35 E	59.09 N	105.60 E	57.58 N
	CLF	Chambon la Foret	France	2.27 E	48.02 N	85.75 E	49.50 N
	TAM	Tamanrasset	Algeria	5.53 E	22.79 N	82.20 E	24.34 N
	MBO	Mbour	Senegal	16.97 W	14.39 N	58.00 E	19.68 N
	CRMN	Cameroon	Cameroon	11.52 E	3.87 N	84.71 E	4.81 N
	CNKY	Conakry	Guinea	13.66 W	9.58 N	60.59 E	14.48 N
Ionosonde	ASC	Ascension	Ascension	14.5 W	7.95 S	57.63 E	2.69 S

Table 2: Am values of the magnetic quiet days used to determine the magnetic quiet reference level

Day	**3/10**	**4/10**	**5/10**	**13/10**	**19/10**	**20/10**	**21/10**	**23/10**	**24/10**	**25/10**	**26/10**	**27/10**	**28/10**
i=	1	2	3	4	5	6	7	8	9	10	11	12	13
Am	1	0	2	2	1	2	2	6	3	5	3	5	4

Figure 1: map of the GPS, the magnetometers and the ionosonde of Ascension Island

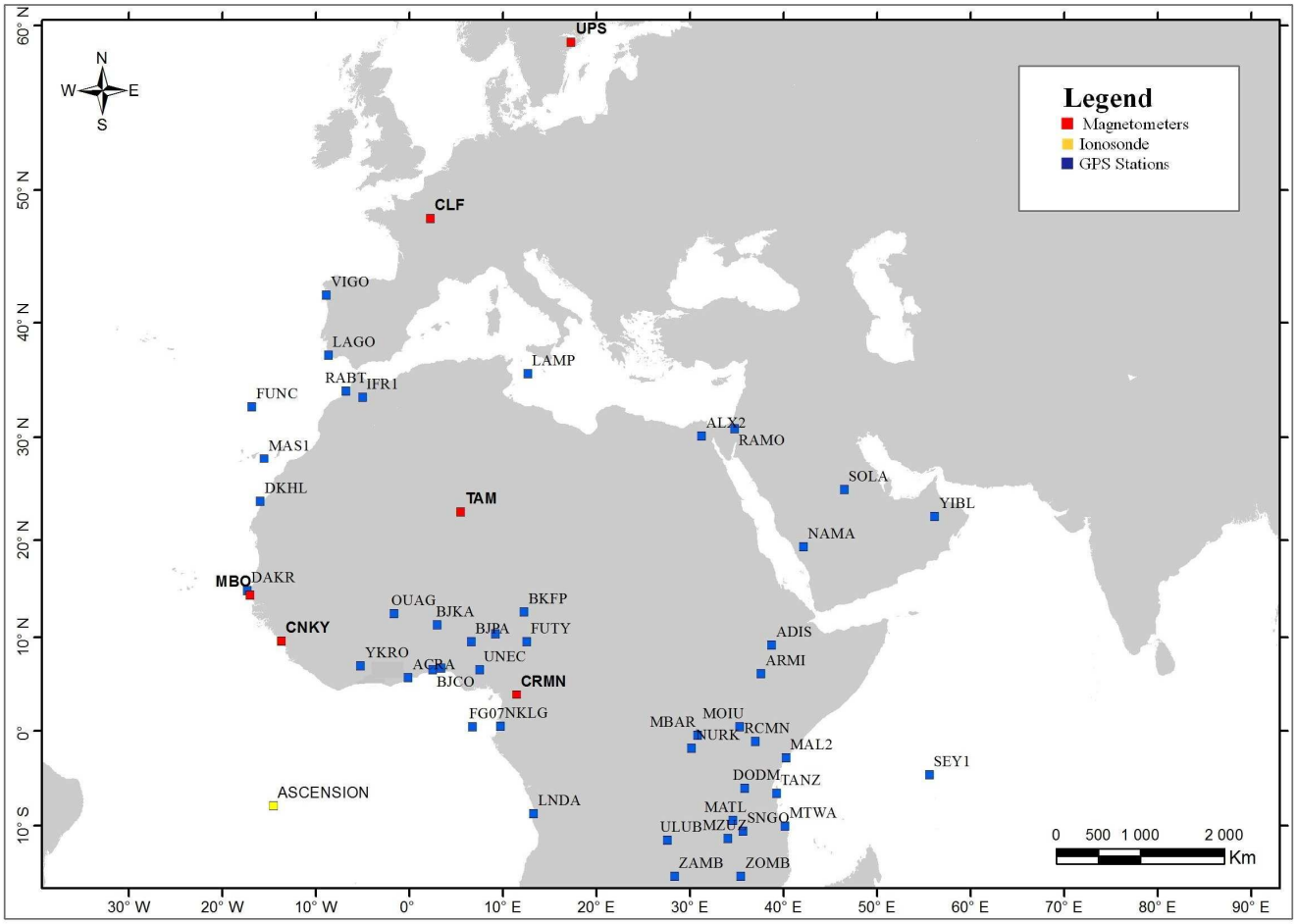

Figure 2 : The solar wind parameters and geomagnetic indices for October 2013: (a) **Vp** the speed of the solar wind in km/s , (b) the **Bz** component of the interplanetary magnetic field, (c) the **Hsym** index and (d) the **AU** and **AL** indices.

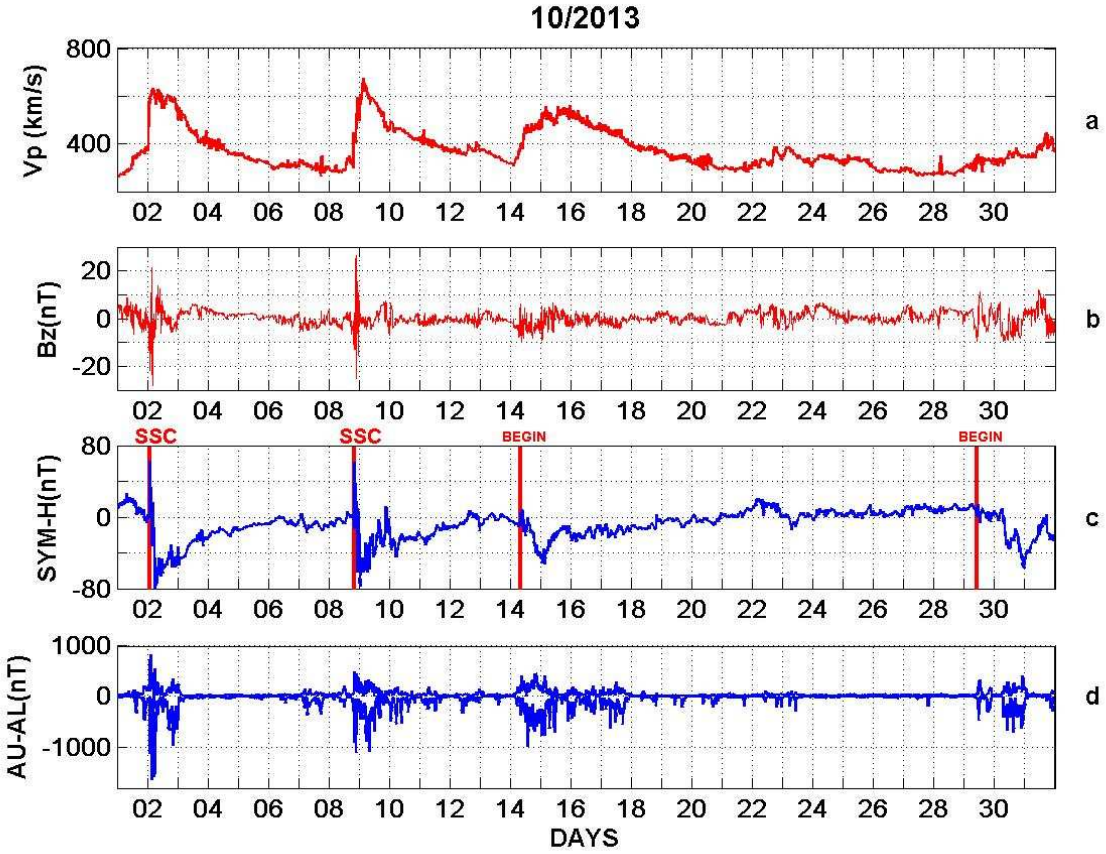

Figure 3 : The solar wind parameters and geomagnetic indices for the 4 selected periods.

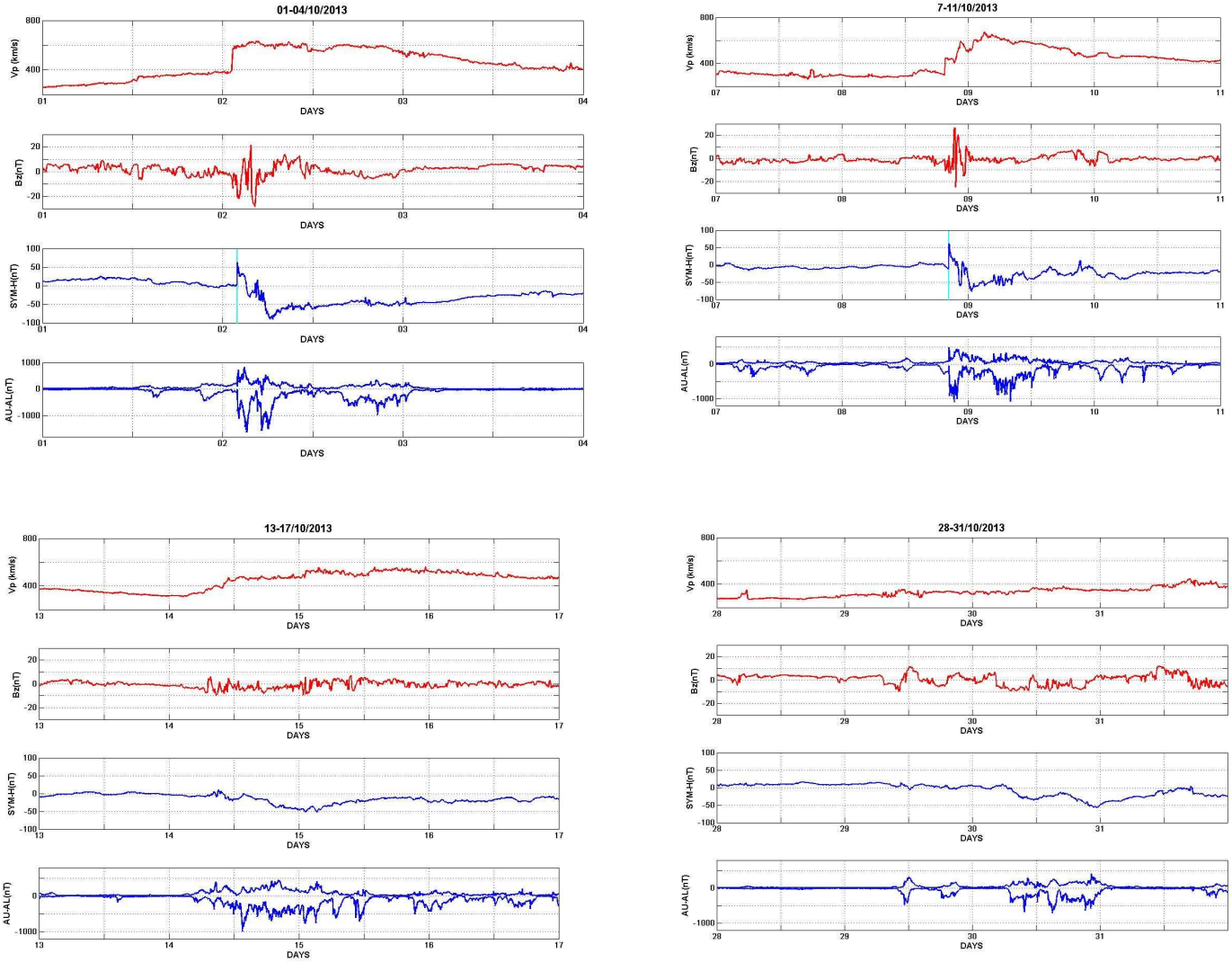

Figure 4a: VTEC along the West-African Europe sector during October 2013

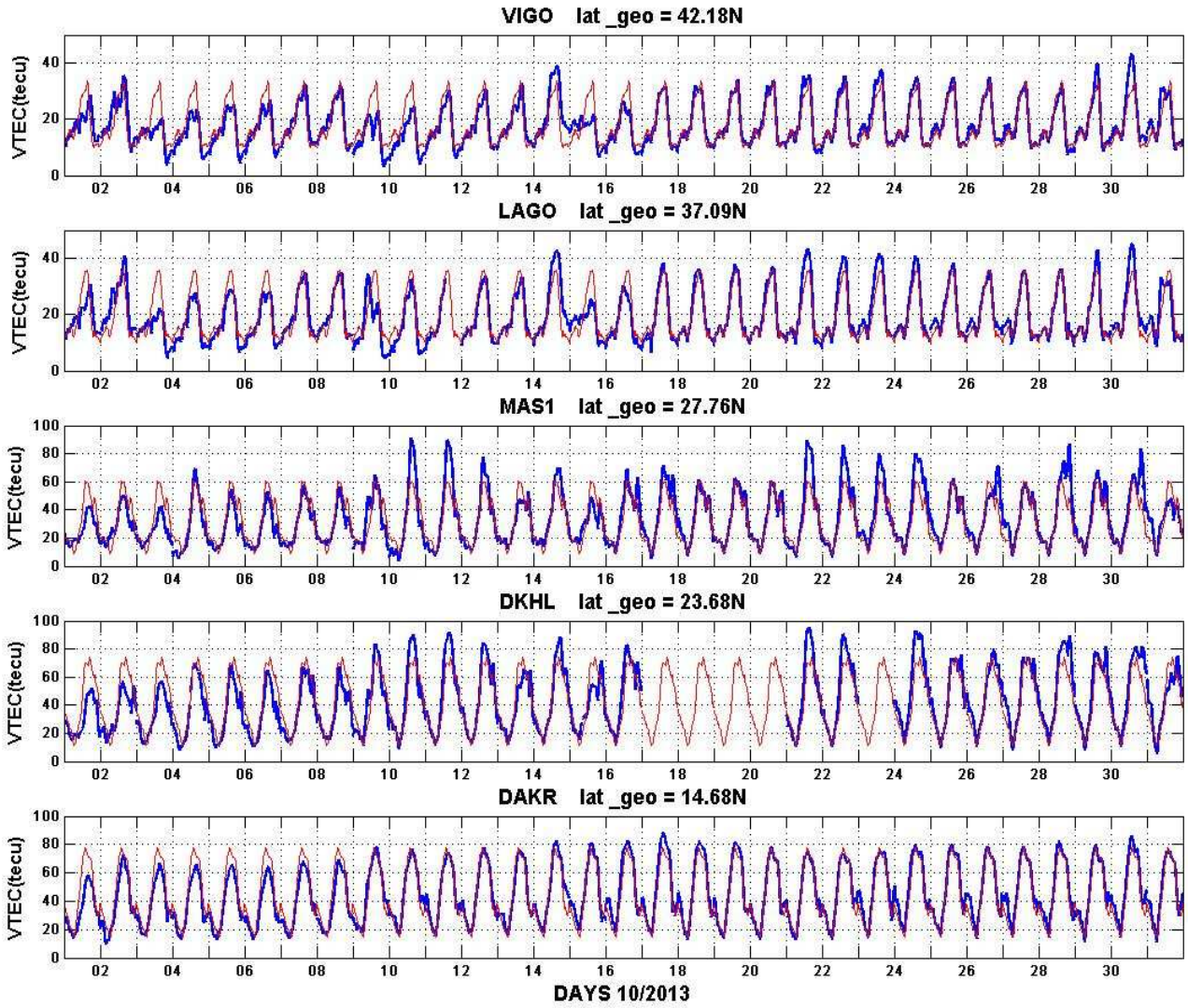

Figure 4b : Daily average deviation of VTEC from the median VTEC

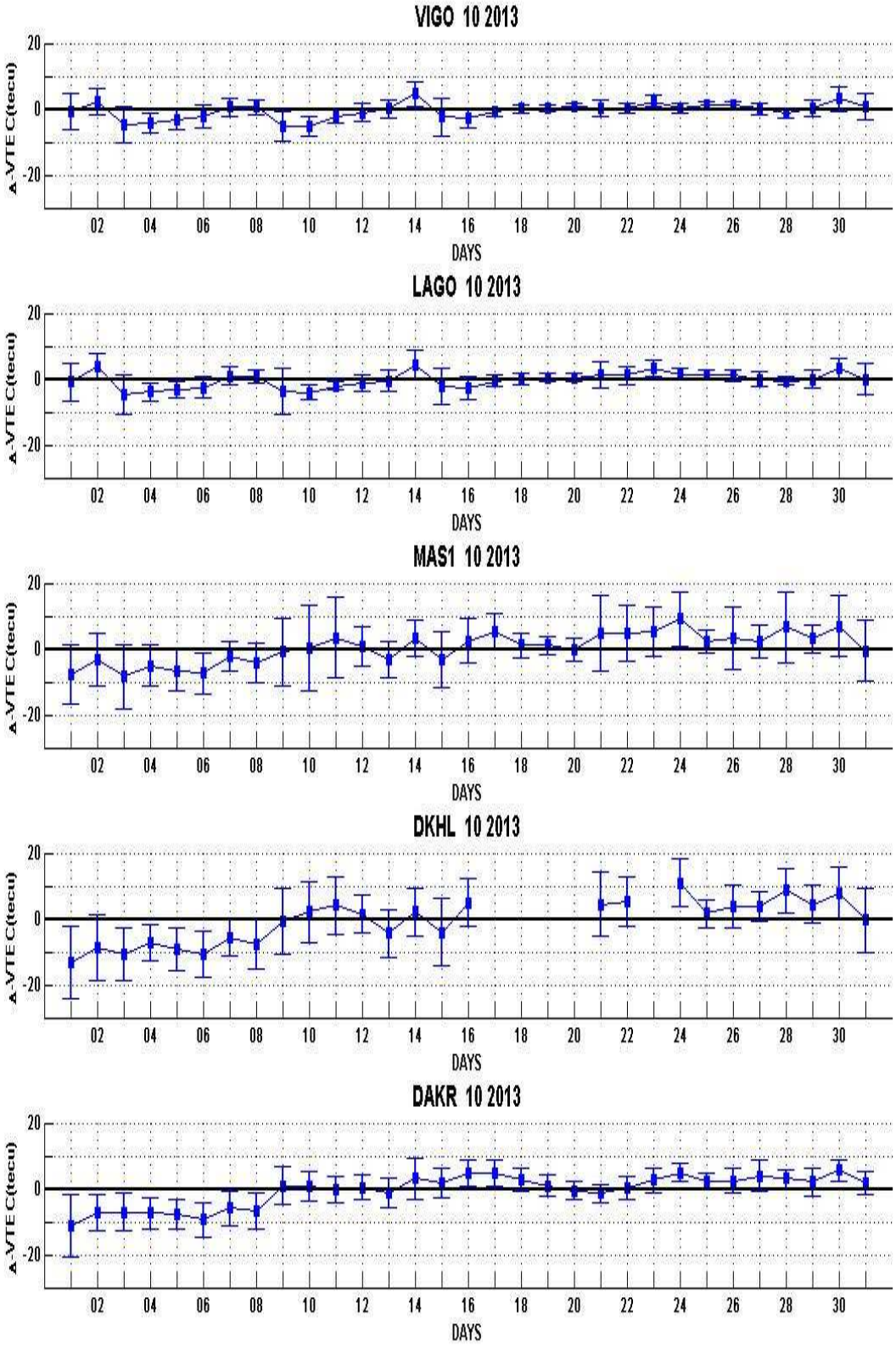

Figure 5 : maps of ROTI index

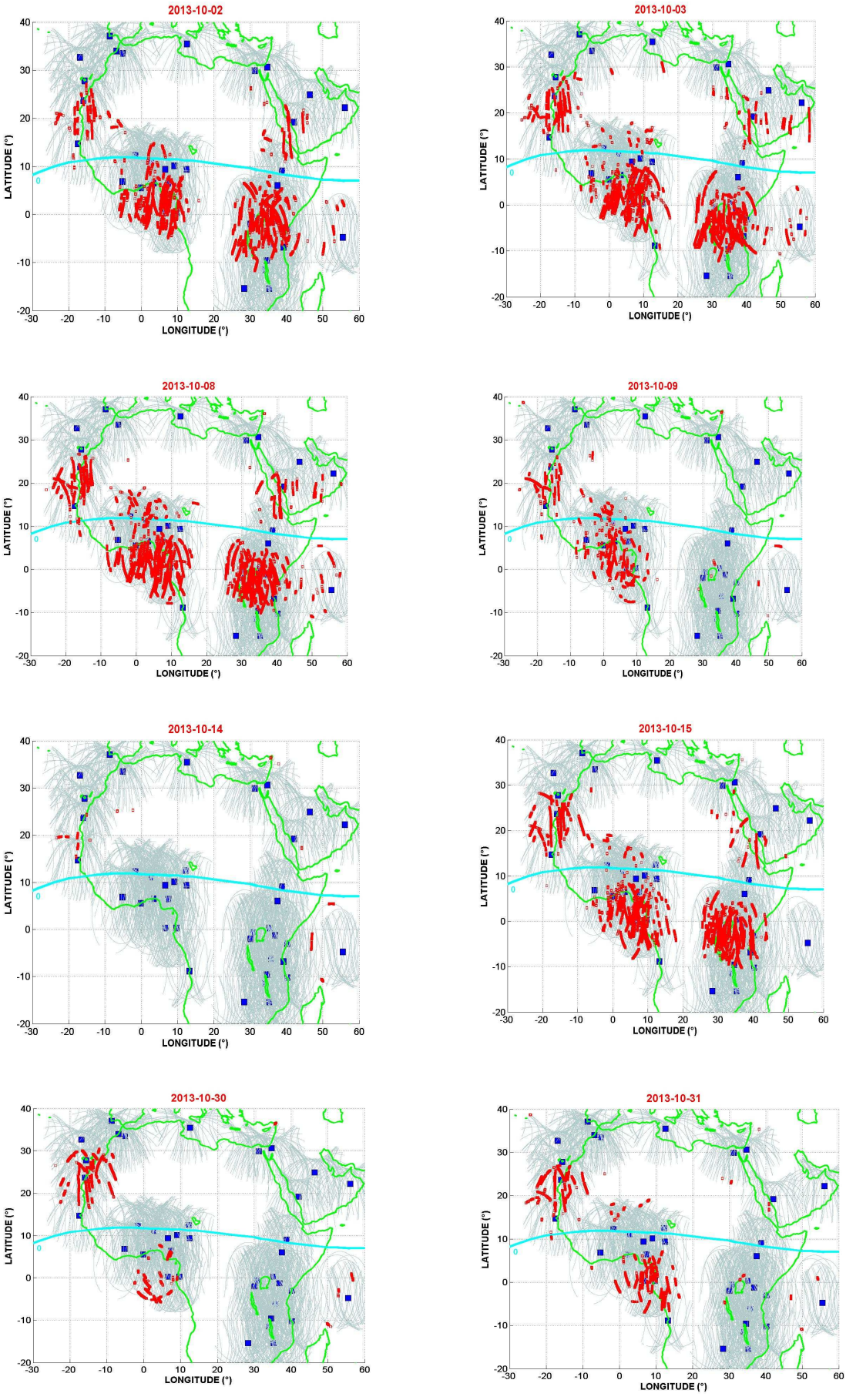

Figure 6: ROTI and Kp indices, along the West-African Europe sector during October 2013

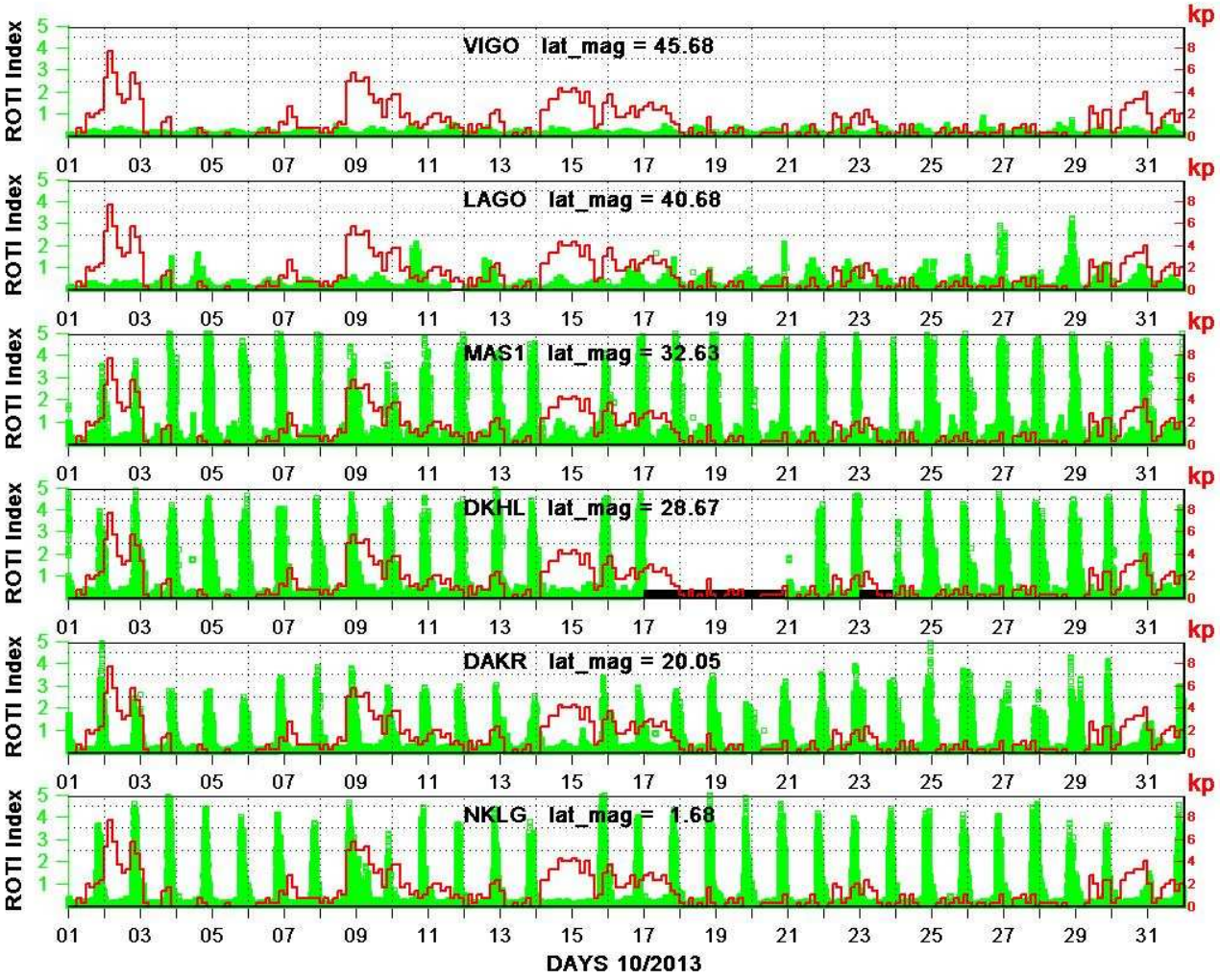

Figure 7 : Ionogram of Ascension Island for 02,08,14 and 30 October 2013, at 22h45 (UT +1)

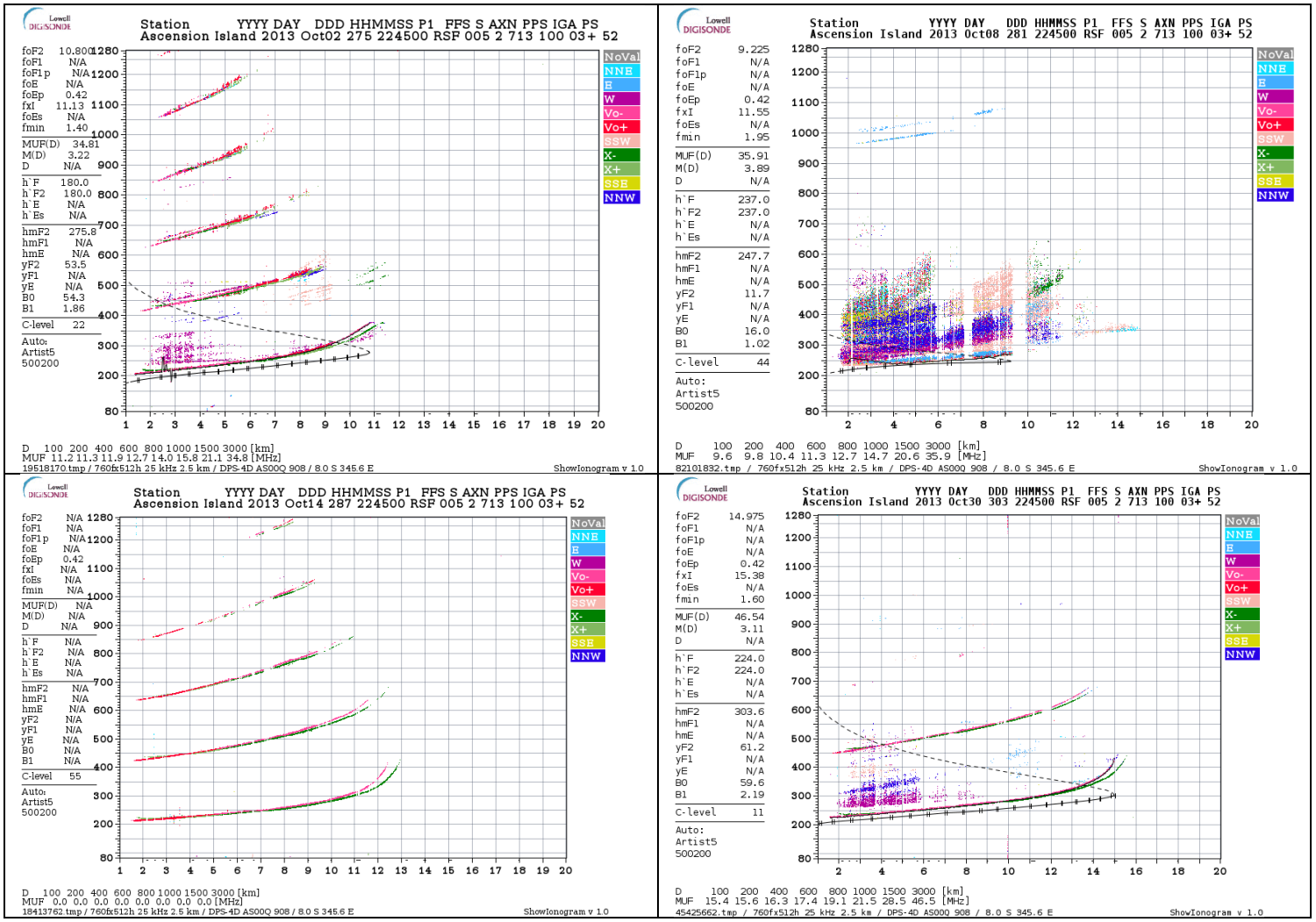

Figure 8 : the variation of the virtual height of the F layer for October 2013, between 15h and 24h, every 15 minutes at 4 MHz in Ascension Island station (UT +1)

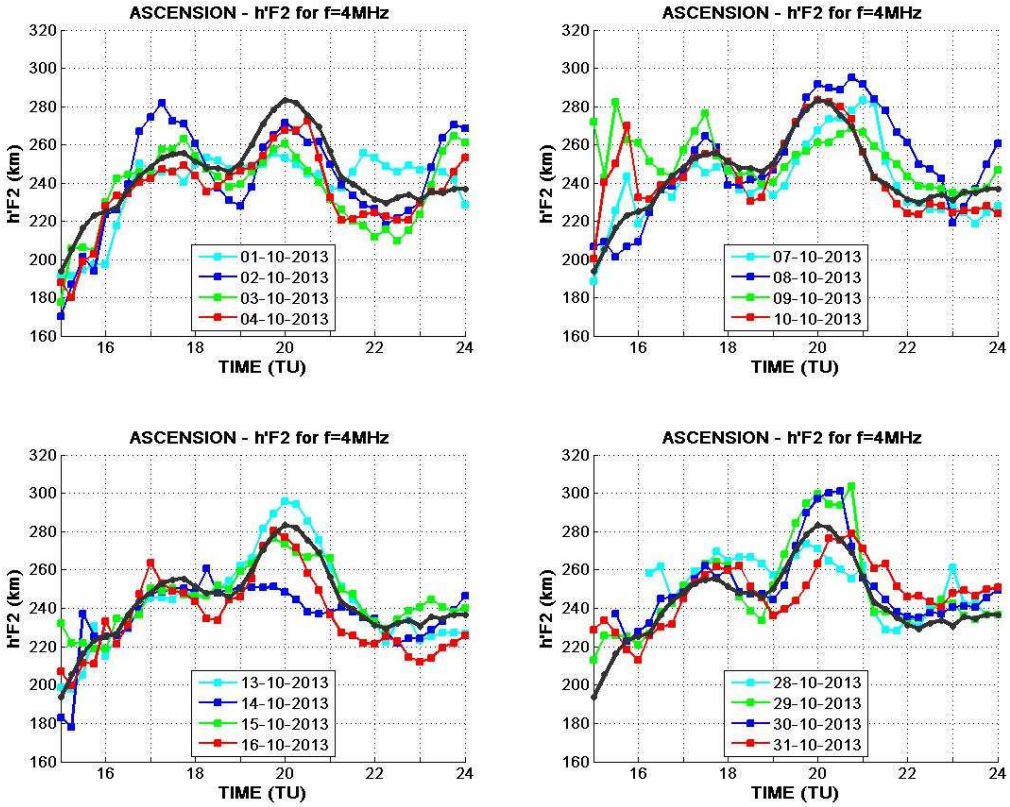

Figure 9: PC and AE indices and H component of the Earth's magnetic field along a latitudinal magnetic chain.

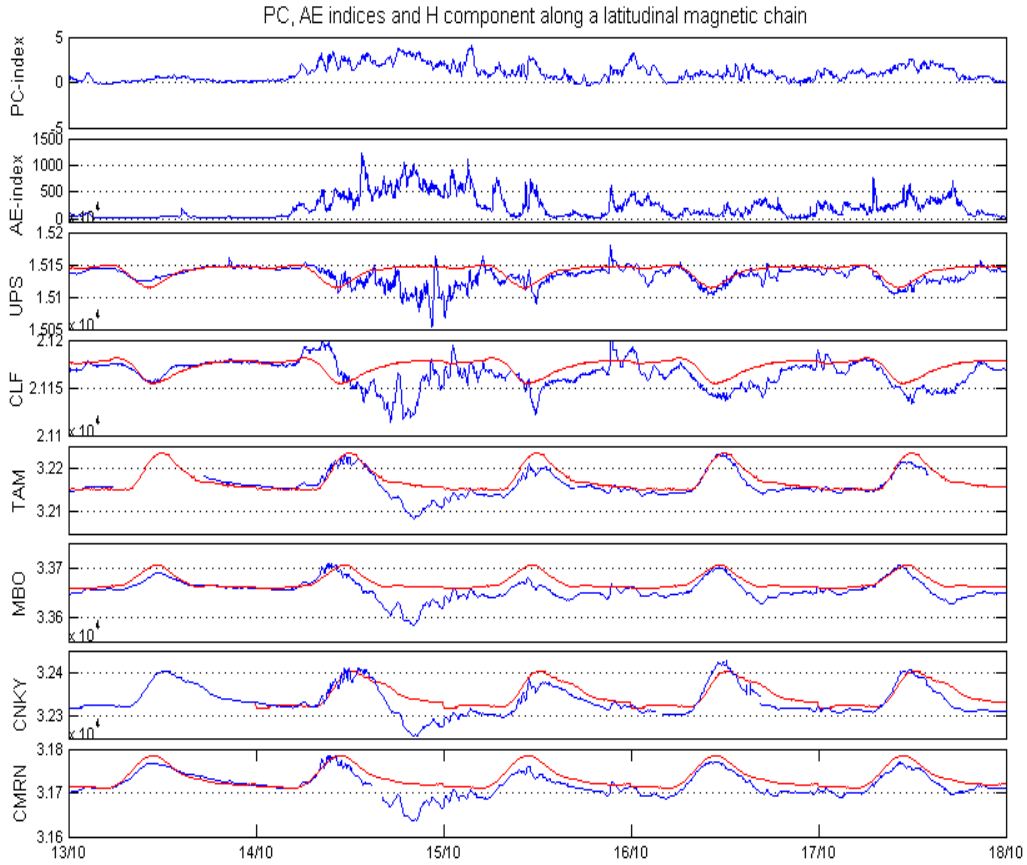

Figure 10 : Disturbances of Ionospheric currents D_{iono} and D_{dyn} at M'BOUR observatory , Senegal

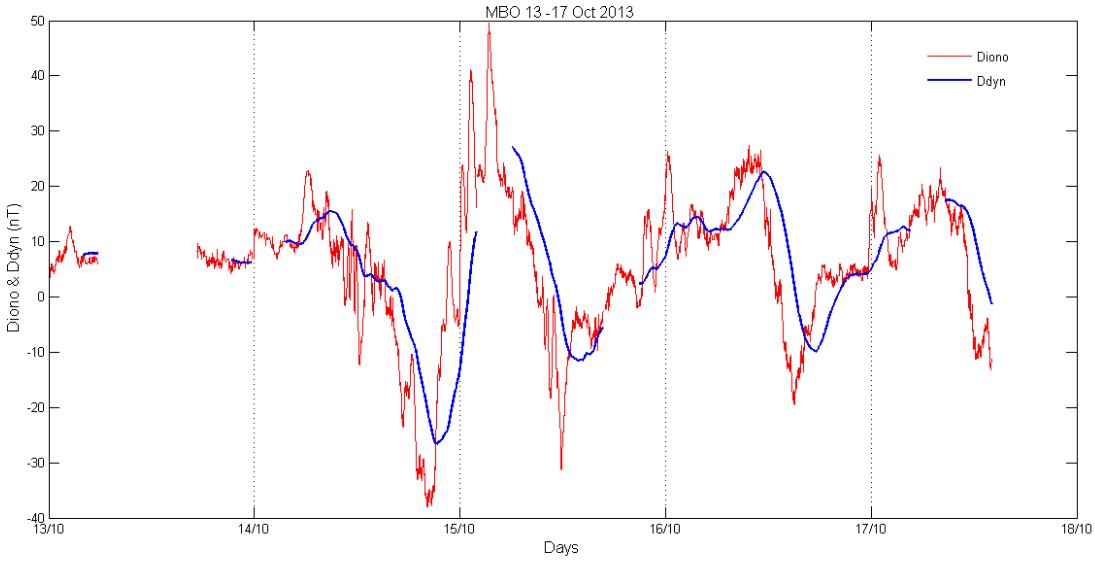

Figure 11 : ROTI and Kp indices, along the East-African-Europe/Middle East sector, during October 2013